Design of a multi-view photogrammetric system based on low cost cameras for the 3D forensic face recognition

Samuele Giuliani [1], Francesco Tosti [1], Pierpaolo Lopes[2], Claudio Ciampini[3] and Carla Nardinocchi [1]*

[1] DICEA, Sapienza University of Rome, samuelegiuliani@gmail.com, f.tosti@live.com
[2] Comando Carabinieri Tutela Ambientale; pierpaolo.lopes@carabinieri.it
[3] Reparto Investigazioni Scientifiche Roma, claudio.ciampini@carabinieri.it

Keywords: low-cost camera, face reconstruction, forensic face recognition, multi-view photogrammetric system.

Abstract:

The manuscript introduces a multi-view photogrammetric system designed to generate detailed 3D facial models to improve forensic face recognition (FFR). Developed in collaboration with the Rome Carabinieri Scientific Investigation Department (RIS), this study represents an initial feasibility study for creating a 3D mug shot with sub-millimetre accuracy utilizing low-cost cameras. To evaluate the system's performance, we conducted three series of experiments. Firstly, virtual environment testing using a 3D digital model to evaluate system performance. Then, real-world setup test using three different camera types to capture the 3D printed 3D model. Finally, some tests in real environment testing with human subjects to assess the ability to handle human skin in real environment. For the first two test, a quantitative analysis of the reconstruction error was performed by measuring the distance between the generated point cloud and the 3D reference model. Using a system based on Raspberry Pi HQ cameras, we obtain an 80% having less then 1 mm of distance from the ground truth. This research demonstrates the potential of low-cost photogrammetry for generating accurate 3D facial models, which could significantly improve the effectiveness of forensic face recognition.

1. Introduction

Three-dimensional facial reconstruction (3DFR) is a key area of interest in fields ranging from gaming entertainment to medical applications such as surgery and orthodontics. In forensic field, police officers have to compare a trace images with a database of mug shot. Typically, 2D mug shot are used that is a front and side view of a person from the shoulder up. Increasingly, trace images derive from surveillance cameras (CCTV) and conventional front and side mug shots can be challenging to compare with CCTV images captured from above. Therefore, the forensic research community are moving away from traditional portrait-based facial recognition methods and looking forward the advantages in using a 3D mug shot that will improve the forensic face recognition (FFR). While techniques using lasers or structured light can achieve sub-millimetre accuracy in creating 3D models, their lengthy acquisition times limit their suitability for 3D facial model reconstruction in non-cooperative context, such as those involving arrested persons (Schippers et. al.,2024). Image-based approaches are the most appropriate method for reconstructing faces in this situation. In recent years, image-based 3D face reconstruction technology has developed rapidly. (Zhang et al, 2024) summarise the main algorithms for 3D facial reconstruction using single or dual image input, such as the front and side images of a traditional mug shot. Among them, methods based on 3D Morphable Model (3DMM) and deep learning have attracted significant research attention. However, even if face recognition is a well-established field, computer vision algorithms are not directly applicable to forensic investigations. Algorithms suitable for forensic applications should satisfy constraints leading to the legal validity of the conclusion during a lawsuit or in the investigation phase (La Cava et.al., 2022). As the FFR represent a mean to determine the strength of evidence in a court of law it has to meet specific requirements. Both the European Network of Forensic Science Institute (ENFSI) and the Facial Identification Scientific Working Group (FISWG) have defined procedure, requirements, approaches to be used for facial recognition. The FISWG provide a list of all the feature for morphological analysis. To illustrate the level of detail, the description of the eyes provided by the manual FISWG is shown. Figure 1 depicts the position of the eyebrow in relation to the position of the eye opening.

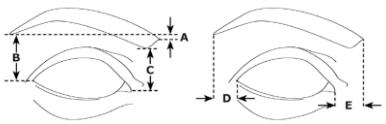

Figure 1. Position of the eyebrow relative to the position of the eye opening (from FISWG)

No specific accuracy is given, but a respect for proportions is required, which may only be guaranteed with an accurate 3D reconstruction that is as close as possible to the real face. Building on the work of La Cava et al. (2022), a photogrammetric approach emerges as the most advantageous method due to its metric accuracy and rapid acquisition time. Prior research demonstrating the feasibility of sub-millimetre accuracy in 3D facial reconstruction using synchronized, high-resolution multi-camera photogrammetric systems (Leipner et al., 2019, 2016; Heike et al., 2010; Lane et al., 2008; Larson et al., 2011; Michienzi et. al., 2018). To the best of our knowledge, the most recent system documented in literature employed 26 synchronized reflex cameras (Leipner et al., 2019). This study investigates the performance of a multi-view photogrammetric system based on low-cost cameras to generate detailed 3D facial models with sub-millimetre precision.

2. Material and method

Three types of experiments were conducted to evaluate the performance of a multi-view photogrammetric system based on low-cost cameras. The first experiment was conducted in a virtual environment using a digital model to assess the system's performance. The second experiments were realized in a real-world setting using three different cameras types to capture the 3D printed model: the Raspberry Module V1, the industrial IDS -USB HQ, and the Raspberry Pi HQ. The last two cameras are compatible with C-mount and CS-mount lenses, and we used the same lens for both. A quantitative error analysis is realized measuring the distance of the reconstructed model to the ground truth. In the initial phase of the study, the 3D reconstruction was performed in an absolute frame defined by the ground control points (GCPs) placed behind the model. This phase involved using two cameras types: the Raspberry Module V1 and IDS-USB camera. A comparison of these low-cost cameras with a high-resolution Sony Alpha 7 reflex camera revealed significant differences in performance. In the second phase, we introduced a newer Raspberry Pi HQ model and shifted to work with a relative frame reconstruction. In fact, the approach of working in an external frame, besides the great disadvantage of not being practicable in the large number of stations where the system should be installed, also presented a lower performance in terms of reconstruction errors. This approach yielded a 3D model that was not scaled or oriented. To assess reconstruction error, we applied a conformal transformation to approximate the model to the ground truth, followed by an Iterative Closest Point (ICP) algorithm using the plugin of the open-software Cloud Compare (Cloud Compare).

It is important to note, that approximate price ratio between the Sony camera and the Raspberry HQ and IDS-USB 3.0 cameras was 10:1 and 5:1, respectively. This is crucial in the forensic field where there is a great interest in producing a more affordable system that guarantees the same accuracy. As an example, in Italy, only the 'Arma dei Carabinieri' has a network of at least 500 systems distributed throughout the country for producing traditional mug shots.

The final experiment was conducted in a real-world setting using human volunteers to evaluate the performance of dense matching on different skin types.

2.1 The 3D model

To evaluate the performance of our multi-image photogrammetric system, we established a reference dataset using a high-resolution 3D digital model (complete with texture information) composed of 954414 triangular meshes. This reference dataset allowed for a quantitative error analysis of the reconstructed model, measured as the distance to the ground truth.

Figure 2. Virtual model and 3D printed model of the 3D virtual model

The virtual model was 3D printed using a Stratasys J750 manufactured by Stratasys (Stratasys). At full scale, this printer has a declared accuracy of up to 0.2 mm for rigid material. The 3D printed 3D model was subsequently captured in a real-world setting. The reconstruction error of the resulting 3D model was measured by comparing it to the original virtual model (*.obj). It's important to note that this error includes the potential inaccuracies introduced during the 3D printing process.

Figure 3. Virtual model and 3D printed model of the 3D virtual model

The reference model enables a point-by-point assessment of the reconstruction error between our reconstructed model and the ground truth.

2.2 Camera configuration in the virtual environment

The virtual environment was initially designed to meet the specific requirements of the RIS investigators. The entire setup, had to be confined to a 2m x 2m area. To achieve this, a 2x2 meter box was modelled in 3DStudio Max. The virtual model was positioned at the centre of this box. Circular targets were placed on three walls: the wall behind the 3D model and the two lateral walls. The distance between the subject and the cameras was maintained at 1.5 meters, which is the standard distance for acquiring 2D mug shots. Next, we wanted a minimum triple coverage of the face and an angle of less than 30 degrees between adjacent cameras to enhance image alignment and subsequent image orientation.

To minimize the number of cameras required, we tested three different field of views (FOV): 80°, 40°, and 20°, while maintaining a constant object distance.

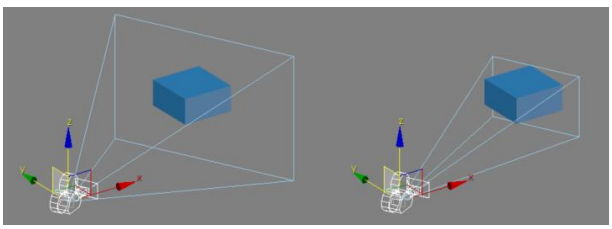

Figure 4. Field of View defined within 3D StudioMax.

The figure illustrates the frames captured by a camera positioned at the same point, but with varying FOVs.

Figure 5. Frame captured at different field of view. (FOV: 80, 40, and 20°)

Initial tests in the virtual environment aimed to determine the optimal field of view. We simulated a reflex camera equipped with various focal length lenses. While a wider field of view could have reduced the number of cameras, it obviously

significantly increased the reconstruction error. Only with the Raspberry Module V1 that has an integrated lens we worked with a large field of view of 55°.
The most basic camera configuration that meets these guidelines is a single row of 8 cameras arranged in a semicircle with a radius of 1.5m, covering a 180° arc.

Figure 6. Image acquisition in the virtual environment.

We used the software Agisoft Metashape ver.1.7 (Agisoft Metashape) to solve the image orientation and image matching step. At first Metashape detects correspondences across the photos, then it applies a greedy algorithm to find approximate camera location and refines them later using a bundle adjustment algorithm to obtain accurate camera position, orientation and distortion parameter. The images alignment is followed by the dense matching (reconstruction stage) whose outcome is the point cloud of the acquired object. All reconstruction errors were calculated using the Cloud-to-Mesh Distance plugin in the open-source software Cloud Compare.

2.3 The cameras

We tested three types of camera: two models of the Raspberry Module V1 (Raspberry Pi V1), the IDS-USN HQ industrial camera (ids-imaging) and the Raspberry Pi HQ (Raspberry Pi HQ). Actually, we only had three cameras for the Raspberry Pi HQ and the IDS-USB HQ, which were moved along the capturing position. We also only had a Raspberry Module V1. This is less than ideal for our multi-view photogrammetric system. However, as we were capturing a static object (the 3D printed 3D model) camera synchronization was not essential in these tests.

	SONY ALPHA 7	IDS	R-V1	R-HQ
Width (px)	6000	2448	2592	4056
Height (px)	4000	2048	1944	3040
W/H	1.50	1.20	1.33	1.33
Width (mm)	35.8	8.446	3.76	6.287
Height (mm)	23.9	7.065	2.74	4.712
Pixel size (μm)	5.9	3.45	1.45	1.55
focal length (mm)	70	16	3.6	16
FOV °(fmax)	28.68	29.57	55.14	30

Table 1. Technical information of the cameras

The industrial IDS USB 3.0 UI-3280CP-C-HQ Rev 2 (Figure 7a) camera is equipped with a Sony 5 MP IMX264 sensor, having a resolution of 2448 x 2048 pixels and a pixel size of 3.45μm. The lens used is a CHIOPT FA1610A with a fixed 16 mm focal length and an image size of 8.4 x 7.1 mm that produce a field of view of about 30°. Table 1 summarise technical information of the three cameras compared with that of a Sony Alpha 7. The Raspberry Pi is a single-board computer running a Linux operating system. The name "Pi" is a reference to Python, the primary programming language used with it. Its success is largely due to its low cost and high performance.

Figure 7. (a) IDS USB HQ; (b) Module V1; (c) Raspberry Pi HQ.

The Camera Module V1 (Figure 7b) connects directly to the Raspberry Pi's connector. It has a resolution of 2592 x 1944 pixel and it mount the Omnivision 5647 sensor provided of a fixed focus lens producing a 55° FOV and a pixel size of 1.45μm. This module connects to the Raspberry Pi, via a 15-pin ribbon cable, to the dedicated 15-pin serial MIPI (CSI) interface, designed specifically for interfacing with cameras.
The Raspberry Pi High-Quality Camera (Raspberry HQ) is based on the Sony IMX477R sensor and has a resolution of 12.3 Megapixel (4056 x 3040). The sensor has a width of 6.287 mm and a pixel size of 1.55 μm. It can operate with exposure times down to 30μs given enough light. Unlike previous models of Raspberry Camera models (Module V1, Module V2, Module 3, and Module 3wide), the Raspberry HQ is compatible with C-Mount and CS-Mount lens.
Camera synchronization is a critical aspect of image acquisition for ensuring sharp, usable images and accurate 3D reconstruction. Two primary methods can be employed: hardware-based and software-based synchronization. The first one is based on a dedicated trigger signal. A central controller sends synchronized trigger signals to each camera, initiating image capture simultaneously. This approach, utilized with the Raspberry Pi HQ cameras, minimizes the risk of motion blur as the entire image is captured at once (Figure 8b). However, it requires specialized hardware and cabling. Software-based synchronization may introduce slight delays, but it can still produce valid results in contexts like face recognition where high-speed, dynamic acquisition is not necessary. Two approaches may be applied. The first consists of setting the internal clock of the cameras simultaneously at the same time and then setting the self-timer. The second one is based on the master-slave configuration. This is the approach used with the IDS cameras (Figure 8a). One camera act as the master, sending synchronization signals to the slave cameras.

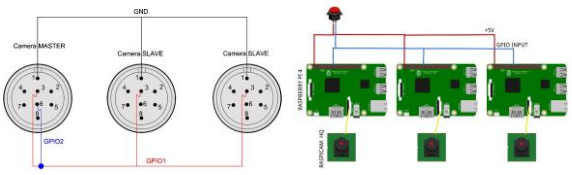

Figure 8. Raspberry Pi Wiring diagram

The TLC IDS camera has a USB 3.0 interface and an 8-pin Hirose and consequently a Hirose HR25-7TR-8PA(73) connector was used. Figure 9 shows the 3 cameras connected. On the left the TLSC IDS and on the right the Raspberry Pi. Finally, an exposure time between 1/500 and 1/1000 seconds is ideal for photogrammetry applications. This helps to minimize

motion blur, especially when dealing with non-cooperative subjects. Figure 8 shows the synchronization scheme of the IDS camera and of the Raspberry cameras.

Figure 9. The three IDS-USB 3.0 cameras and the three Raspberry Pi HQ cameras.

3. Results

3.1 Virtual environment

The 3D model, defined within the 3D world frame established in the virtual room, was captured using 8 cameras. Each camera acquired an image from a unique position, defining a 3D camera frame with its origin at the camera's projection centre and its z-axis aligned with the camera's optical axis. The external parameters, consisting of the three coordinates of the projection centre in the 3D world frame and the three rotations required to align the 3D camera frame with the 3D world frame, define the 6 camera orientation parameters. These parameters establish the relationship between the 3D world frame and the individual camera frames. In practice, the true orientation parameters were obtained from 3DStudio Max, where the cameras were positioned in the virtual scene. These parameters were imported into Agisoft using the *.abc format, enabling interoperability between the two software.

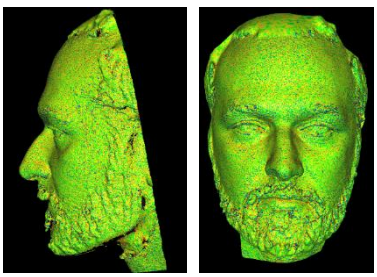

Figure 10: Reconstruction error superimposed the 3D model. Error between ±0,02 mm represented in green; error up 0,1 mm in red and error down to -0,1 mm in blue.

This test represents a benchmark, showing the theoretical limit achievable with the reconstruction process, as the error is solely dependent on the camera network and dense matching algorithm. Figure 10 shows the reconstruction errors visually represented as a colour map overlaid onto the 3D model, providing a clear visualization of error distribution across the facial surface. Results show a mean value equal to 0 and standard deviation of 0.2mm. This value is the noise level we have in the reconstruction. It can overlay the noise of the 3D printer. Because our aim is a maximal error of 5-10 mm we can neglect the effect of the printer. The last test in the virtual environment was to evaluate the reconstruction error working through an absolute orientation or a relative orientation. In this last case, a scale bar is used to scale the reconstructed 3D model.

3.2 Real setting with 3D printed 3D model

Using an 8-camera configuration we capture the 3D model with the Sony Alpha 7 cameras with a field of view of 28.68°.

Figure 11. Reconstruction error of Sony Alpha 7 camera superimposed the 3D model. All the errors are within 1mm.

The standard deviation of the reconstruction error is equal to 0.7mm and 100% of the points have an error of less than 1mm, confirming the valid performance of such a high-resolution camera even with an 8-cameras configuration.

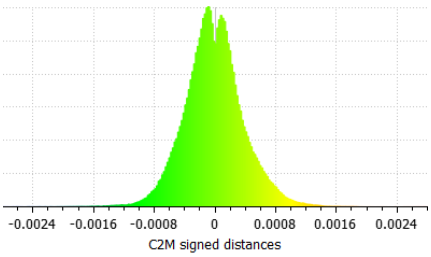

Figure 12. Reconstruction errors distribution with 8 acquisition of Sony Alpha 7 camera.

Figure 12 shows the histogram of the reconstruction error. The figure 13 shows the reconstruction error superimposed to the 3D model of the Raspberry Module V1 (on the left) and of the IDS-USB camera (on the right). The Module V1 3D model presents large error up to 2.98mm around the nose and a standard deviation of 1mm. The figure 14 reports the distribution of the reconstruction error. The IDS-USB 3D model presents errors up to 15mm. The figure 15 shows the error distribution.

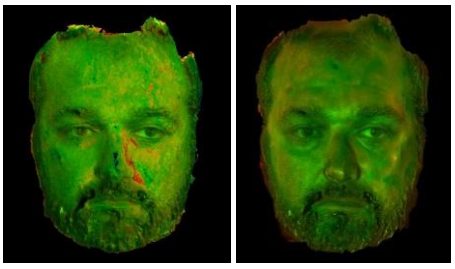

Figure 13. Reconstruction error superimposed the 3D model.

In the second phase of this study we tested the Raspberry Pi HQ working in a relative frame. Moreover, to improve the results of such low-cost cameras we increased the number of cameras adding a cameras row above and below the initial row, creating in such a way both side and lateral overlap.

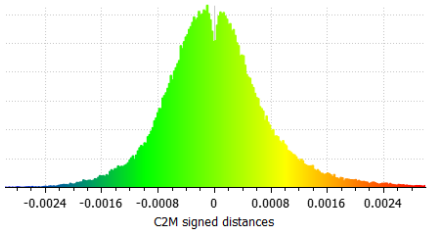

Figure 14. Reconstruction errors distribution with 8 acquisition of the Module V1 camera.

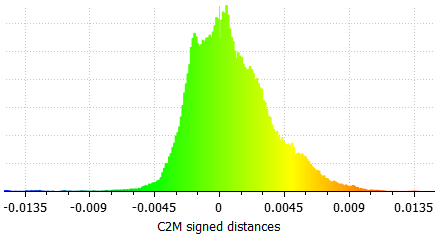

Figure 15. Reconstruction errors distribution with 8 acquisition of the IDS-USB camera.

Additionally, due to practical considerations involving the repositioning of three connected cameras we add 1 additional camera to each row defining a final 27 cameras configuration. Figure 16 shown the configuration with the 27 cameras.

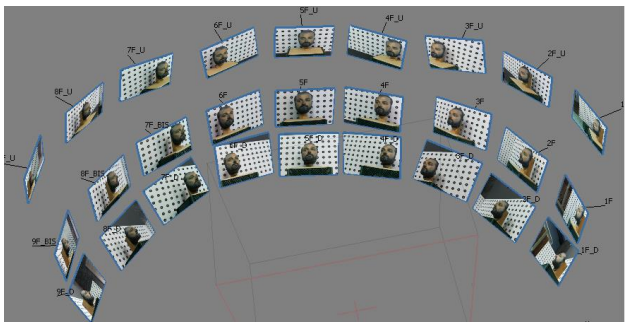

Figure 16. The 27 camera configurations used with Raspberry Pi HQ.

The cameras in the additional rows were tilted of 18° along the x-axis downwards for the cameras in the row above the first and upwards for the cameras in the row below. The 3D model was scaled within Agisoft Metashape using a known distance (scale bar) selected between two background GCPs and aligned by the Iterative Closest Point (ICP) plugin of Cloud Compare. Two distinct models were produced: the first scaled using a single distance scale (Figure 17), and the second scaled applying a scale factor estimated through ten known distances (Figure 18).

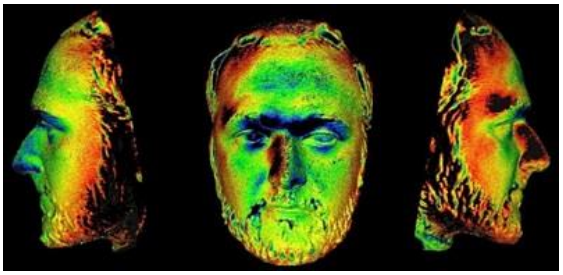

Figure 17. Reconstruction errors overlaid on the 3D model using 27 camera configurations and scaling the model with one known distance.

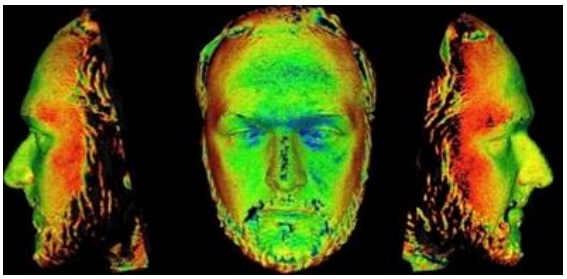

Figure 18. Reconstruction errors overlaid on the 3D model using 27 camera configurations and scaling the model ten known distance.

Figure 19 shows the histogram of the reconstruction errors within the range from -5 mm to 5 mm. The blue figure plot shows the error of the model scaled with a single distance of approximately 60 cm in length, whereas the orange figure plot describes the error of the model scaled with the scale factor estimate using 10 known distances, each with a mean length of 60 cm.

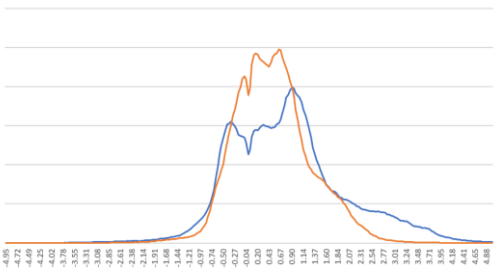

Figure 19. Error distribution in the range from -5 mm to 5 mm for the model scaled with one single distance (blue figure) and with 10 distances (red figure).

The standard deviation of the errors for the model scaled with a single distance is 1.4 mm, whereas it is 0.9 mm for the model scaled using 10 distances. Furthermore, 80% of the points in the model scaled with 10 distances have a distance from the reference model within ±1 mm, compared to 65% in the model scaled with a single distance.

https://doi.org/10.5194/isprs-archives-XLVIII-2-W8-2024-177-2024

3.2 Real setting with volunteers

Despite the lack of synchronization among all the frames, since we took all the image in sequence with the relocation of the cameras to cover all the angles, we successfully obtained the 3D models for four volunteers who maintained their positions throughout the acquisition process. The volunteer's collaboration allowed us to verify the performance of dense matching on real subjects, which is influenced by camera resolution. For one of them we produced a complete satisfactory 3D facial model. It's important to emphasise that in this last test, used a full configuration of 27 cameras, synchronized for three. That means that the three cameras were relocated 9 times to acquire the 27 shots.

Figure 20. Frontal pose of the 3D model and frontal images acquired with the Sony Alpha 7 camera.

Only a qualitative analysis was possible with these last tests, therefore the results could only be analysed through visual analysis. The first volunteer was captured with the Sony Alpha 7 camera acquiring 8 frames. Figure 20 shown on the left the 3D model in a frontal view that can be compared with the frontal images of the volunteer.

Figure 21. Frontal pose of the 3D model and frontal images acquired with the Raspberry Module V1.

The second volunteer was captured with eight frames of the Raspberry Module V1. The 3D model shows the reconstruction is incomplete, but the software aligned and oriented all eight images.

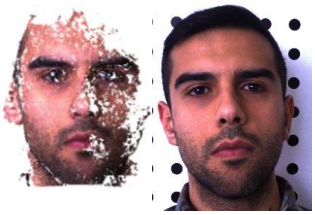

Figure 22 Frontal pose of the 3D model and frontal images acquired with the IDS-USB 3.0 HQ

The third volunteer was captured with eight frames of the IDS-USB 3.0 HQ. The model is still incomplete, but this is less of an issue than before. This camera shows better performance than the Raspberry Module V1.
The last volunteer was acquired with the Raspberry Pi HQ camera using 18 cameras. It was not possible to keep the position with 27 no-synchronised cameras but a complete 3D model was made anyway.

(a) (b) (c)

Figure 23. Frontal pose of the 3D model (a) and frontal images (b) acquired with the Raspberry Pi. (c) lateral pose with texture.

The small not reconstructed area was resolved with the texture overlaid, as shown in Figure 23c to the meshed model. It is not possible for large hole as in the model of Figure 20, Figure 21, and Figure 22. The 3D mug shot allow to generate different pose (Figure 24) of the subject according to the trace images to match.

Figure 24. Frames extracted from the 3D model to improve face recognition.

4. Conclusion

Research in the forensic context is driving the adoption of 3D data from emerging technologies. To ensure the admissibility of such evidence, morphological features must be accurately preserved, and metric measurements must be precise.
Advances in forensic facial recognition and 3D mugshot technology aim to enhance their evidentiary value and legal acceptance. This necessitates rigorous approaches to face reconstruction.
This study tested three low-cost camera types. Our results indicate that cameras with reduced fields of view, due to their sensor dimensions, require a three-row camera configuration to produce a robust image bundle oriented in a relative frame. This study proposes a multi-view photogrammetric approach using low-cost Raspberry Pi HQ cameras to create high-precision 3D mugshots with submillimetre accuracy. Specifically, we obtained that, 80% of the points have a distance of less than ±1

mm when multiple scale bars are used to estimate the scale factor.
Having a 3D model of a suspect's face would allow forensic experts in facial recognition to improve the alignment of the known face with anonymous images captured by CCTV (Giuliani et.al., 2024). In reality, the images of a subject to be identified are rarely taken from a frontal or profile view. Surveillance cameras mainly capture people from above and this factor can be decisive in investigations.

References

Agisoft Metashape (ver 1.7) www.agisoft.com (last access on 29.07.2024)

Botscan by Botspot, https://botspot.de/botscan-neo/ (last access on 24.07.2024)

CloudCompare (version 2.13) [GPL software]. (January 28, 2024). Retrieved from http://www.cloudcompare.org/ (last access on 04.11.2024)

ENFSI. Best Practice Manual for Facial Image Comparison. ENFSI-BMP-DI-01. Version 01 – January 2018.

FICWG. Facial Image Comparison Feature List for Morphological Analysis. Version 2.0, 2018.09.11.

Giuliani, S., Tosti, F., Lopes, P., Ciampini, C., Nardinocchi, C., 2024. Design of a Multi-Vision System for a Three-Dimensional Mug Shot Model to Improve Forensic Facial Identification. *Applied Science* 14, 9285. doi.org/10.3390/app14209285

Heike, C. L., Upson, K., Stuhaug, E., Weinberg, S.M., 2010. 3D digital stereophotogrammetry: a practical guide to facial image acquisition. *Head Face Med.*, 6-18. doi.org/10.1186/1746-160X-6-18

IDS-imaging, https://en.ids-imaging.com/store/u3-3280se-rev-1-2.html. (last access on 05.11.2024)

La Cava S., Orrù, G., Goldmann, T., Drahansky, M., Marcialis, G.M., 2022. 3D Face Reconstruction for Forensic Recognition – A Survey. *26th Intern. Conf. on Pattern Recognition (ICPR)*, August, 21-25, Montreal, Quebec, Canada. doi.org/10.1109/ICPR56361.2022.9956031

Lane C., Harrel, W. Jr., 2008. Completing the 3-dimensional picture. *American Journal of Orthodontics and Dentofacial Orthopedics*, Vol. 133, Issue 4, April, 612-620. doi.org/10.1016/j.ajodo.2007.03.023

Leipner A., Obertová, Z., Wermuth, M., Thali, M., Ottiker, T., Sieberth, T., 2019. 3D mug shot—3D head models from photogrammetry for forensic identification. *Forensic Science International*, 300 (2019), 6-12. doi.org/10.1016/j.forsciint.2019.04.015

Larson B.E., Leona, V., Beiraghi, S., 2011. Accuracy and precision of a 3D anthropometric facial analysis with and without landmark labelling before image acquisition. *Angle of Orthodontist*, Vol. 81, No.2, March, 245-52. doi.org/10.2319/041810-210.1

Michienzi R., Meier, S., Ebert, L. C., Martinez, R. M., Sieberth, T., 2018. Comparison of forensic photo-documentation to a photogrammetric solution using the multi-camera system "Botscan". *Forensic Science International*, 288, 46-52. doi.org/10.1016/j.forsciint.2018.04.012

Rasberry Pi HR: https://www.raspberrypi.com/products/raspberry-pi-high-quality-camera/ (last access on 05.11.2024)

Raspeberry Pi Module V1: https://www.raspberrypi.com/documentation/accessories/camera.html (last access on 05.11.2024)

Schipper, J.A.M., Merema, B.J., Hollander, M.H.J., Spijkervet, F.K.L., Dijkstra, P.U., Jansma, J., Schepers, R. H., Kraeima, J., 2024. Reliability and validity of handheld structured light scanners and a static stereophotogrammetry system in facial three-dimensional surface imaging. *Scientific Reports*, 14(1), April.doi.org/10.1038/s41598-024-57370-x.

Stratsys: https://pdf.aeroexpo.online/pdf/stratasys-gmbh/j750-spec-sheet/170653-5605-_3.html (last access on 12.07.2024)
3DStudioMax: autodesk.com/products/3ds-max/features (last access 29.07.2024)

Zhang, B., Li, Y., Li, X.,Liu, D., Li, Z., Sun, X., 2024. A Review of Research on 3D Face Reconstruction Methods *ICIIT '24: Proc. 9th Intern. Conf. on Intelligent Information Technology*, 70 – 76. doi:10.1145/3654522.3654534

Xangle Studio. URL: https://xangle3d.com (last access on 24.07.2024)

3dMD Application: https://3dmd.com (last access on 24.07.2024)